Wookju Jang[1,2]*
Jaesool Shim[2,3]*
Dong-Yeon Lee[2,3]
Prashanta Dutta[4]
Jae-Ryong Kim[5]
Kyung-Hyun Cho[1,2]

[1]School of Biotechnology, Yeungnam University, Gyeongsan, Republic of Korea
[2]Research Institute of Protein Sensor, Yeungnam University, Gyeongsan, Republic of Korea
[3]School of Mechanical Engineering, Yeungnam University, Gyeongsan, Republic of Korea
[4]School of Mechanical and Materials Engineering, Washington State University, Pullman, USA
[5]Department of Biochemistry and Molecular Biology, Aging-associated Vascular Disease Research Center, Yeungnam University, Daegu, Republic of Korea

Received July 5, 2011
Revised September 4, 2011
Accepted September 24, 2011

Research Article

Rapid detection of dysfunctional high-density lipoproteins using isoelectric focusing-based microfluidic device to diagnose senescence-related disease

Recently, we reported elevated levels of advanced glycated end products (AGEs) in human high-density lipoproteins (HDL), with fragmentation of apoA-I in an elderly group, compared with a younger group. More dysfunctional HDL from human plasma was demonstrated in the elderly group, including reconstituted HDL containing glycated apoA-I (gA-I-rHDL) with elevation of AGEs. Based on SDS-PAGE analysis, HDL_3 from the elderly group (E-HDL_3) exhibited increased multimerization with increased smear band intensity compared to HDL_3 from the younger group (Y-HDL_3). According to isoelectric focusing gel analysis, gA-I-rHDL and E-HDL_3 showed electromobility to the basic region of pH with a broader band range. In a microfluidic channel, E-HDL_3 had faster mobility with a broader range and a higher isoelectric point (p*I*, approximately 8.1), whereas Y-HDL_3 showed a narrow band range with a lower p*I* (approximately 6.9). In conclusion, gA-I-rHDL and E-HDL share several electrophoretic properties with multimerization and faster mobility in microfluidic channels, depending on the isoelectric point. These results can be applied to develop a rapid detection system for modified HDL to predict the extent of aging and aging-related metabolic diseases, such as cardiovascular disease and diabetes.

Keywords:
Aging / Apolipoprotein A-I / High-density lipoproteins / Isoelectric point / Microfluidics
DOI 10.1002/elps.201100361

1 Introduction

It is well-known that plasma high-density lipoprotein-cholesterol (HDL-C) levels are inversely correlated with the risk of cardiovascular disease (CVD) [1]. HDL ($1.063 < d < 1.225$) is a complex of apolipoprotein and lipid in plasma. HDL plays a critical role in reverse cholesterol transport (RCT), which is involved in the removal of excess cholesterol from peripheral cells and delivery to the liver and steroidogenic cells for catabolism [2]. HDL has subtypes, depending on the density and size, such as HDL_2 and HDL_3. In healthy state, especially in young athletes' plasma, HDL has more potent antioxidant ability with larger particle size than in sedentary controls [3]. As well as CVD, HDL-cholesterol is directly related to healthy aging [4] and the longevity syndrome [5]. These reports suggested that HDL and HDL-C exert anti-atherosclerotic and anti-senescence activities [6]. However, the beneficial HDL can be degenerated to a dysfunctional HDL, which has pro-atherosclerotic and pro-inflammatory molecules, by several modifications with aging or acute stress, including oxidation [7], glycation [8] and enzymatic cleavage, such as matrix metalloproteinase [9]. Interestingly, HDL from aged subjects showed increased sensitivity of oxidation induced with age by γ-radiolysis of water [10], indicating more production of dysfunctional HDL with age.

We have also shown that HDL, especially HDL_3, possesses stronger anti-inflammatory and anti-aging activities than HDL_2 [11] and exerts more potent antioxidant and anti-inflammatory effects than HDL_2 [12]. Additionally, we reported that alteration of HDL occurred during both acute inflammatory phase [13] and chronic metabolic disease, such as the metabolic syndrome [14]. Furthermore, several functional and structural changes were detected in plasma of the elderly; specifically, loss of antioxidant ability, cleavage of apoA-I, reduction of HDL particle size, and increase in advanced glycated end products were associated with aging, as well as an undesirable change in the serum lipid

Correspondence: Professor Kyung-Hyun Cho, School of Biotechnology, Yeungnam University, Gyeongsan 712-749, South Korea
E-mail: chok@yu.ac.kr
Fax: +82-53-814-3026

Abbreviations: AGE, advanced glycated end product; **HDL,** high-density lipoproteins; **HDL-C,** high-density lipoprotein cholesterol

*These authors contributed equally to this work.

Colour Online: See the article online to view Figs. 2–7 in colour.

© 2011 WILEY-VCH Verlag GmbH & Co. KGaA, Weinheim

profile. Reconstituted HDL-containing apolipoprotein A-I (apoA-I), phospholipid and cholesterol have been synthesized to mimic normal HDL in serum. Glycation of the rHDL could mimic HDL from the elderly (E-HDL), which was more glycated and oxidized, as demonstrated in our previous report [11, 15].

The electromobility of protein is greatly influenced by the change in the electric charge of the protein and the isoelectric point (p*I*). We recently reported that the elderly (71 ± 4 years, $n = 26$) showed remarkably different functional and structural properties of HDL, compared with a young group (22 ± 2 years, $n = 18$). HDL from the elderly group showed loss of antioxidant ability, cleavage of apoA-I and reduction of HDL particle size [15]. These results strongly suggest that modification of HDL can influence electromobility and can therefore serve as a biomarker for aging.

IEF is one of most reliable and useful separation techniques for charged amphoteric species, such as proteins, DNA, RNA and peptides under an electric field. Although amphoteric species can be separated by the size, shape, charge, weight and hydrophobicity, IEF is used by charge due to its high resolution and applicability to a broad range of applications, from single charged molecules (such as DNA) to macromolecules and living cells. In IEF, amphoteric compounds migrate with their different mobilities in a pH gradient generated by a variety of ampholytes, and are concentrated, focused and isolated at unique p*I*s at which molecules have a zero net charge.

Recently, the emergence of nanoelectromechanical system (NEMS)/microelectromechanical system (MEMS) technology has been driven for IEF in microfluidic devices due to its fast results, and low sample requirements and reagent consumption [16–18]. In 2002, Tan et al. demonstrated miniaturized capillary isoelectric focusing using plastic microfluidic devices. The total analysis time was only 150 s for focusing in a 1.2 cm-long plastic channel (50 μm deep × 120 μm wide) [16]. In addition, in 2003, Sia et al. developed the very well-known poly (dimethylsiloxane) (PDMS), which is very easy for micro-fabrication, and introduced PDMS-based micro-devices for immunoassays, separation of proteins and DNA [17]. In 2004, Li et al. introduced the plastic microfluidic network which is available for multidimensional protein separations [18].

There have been numerous reports regarding IEF based on chip and capillary analysis of macromolecules, such as blood proteins, to detect progress of various diseases, as reviewed by Shimura [19]. For further application of bioparticles, various capillary and chip electrophoresis methods have been developed for detection of viruses, organelles and cells [20]. To the best of our knowledge, however, there has been no report on methods to detect modified proteins, either structurally or functionally, to compare between healthy state and disease state. Recently, Liu group reported a micellar electrokinetic chromatography (MEKC) method to analyze HDL phospholipids [21]. Although the method was simple and fast, it has a limitation in that it can analyze phospholipid, but not HDL particle itself. So far, there has been no detection method to compare electromobilities between normal HDL and dysfunctional HDL using Lab-on a chip.

In order to rapidly detect the extent of senescence and the onset of senescence-related disease, we compared electromobility of various HDL subtypes on IEF gel and microfluidics based on IEF, using poly-dimethyl siloxane (PDMS) microchips and ampholyte.

2 Materials and methods

2.1 Materials

ApoA-I was purified from human plasma using ultracentrifugation, column chromatography and organic solvent extraction, following the method described by Brewer et al. [22]. The purified apoA-I was lyophilized at −80°C until use. 1-Palmitoyl-2-oleoylphosphatidylcholine (POPC, cat 850457C) was purchased from Avanti Polar Lipids (Alabaster, AL, USA). Cholesterol (C8667) and sodium cholate (C1254) were obtained from Sigma (St. Louis, MO, USA).

2.2 Isolation of HDL from elderly and young groups

Very low-density lipoprotein (VLDL; $d < 1.019$ g/mL), LDL ($1.019 < d < 1.063$), HDL_2 ($1.063 < d < 1.125$) and HDL_3 ($1.125 < d < 1.225$) were isolated from the sera of elderly (mean age 71 ± 4 years, $n = 26$) and young male subjects (mean age 22 ± 2 years, $n = 18$), via sequential ultracentrifugation, with the density appropriately adjusted by addition of NaCl and NaBr, as detailed in our previous report [23], and is in accordance with standard protocols [24]. Samples were centrifuged at $100{,}000 \times g$ for 24 h at 10°C, using a Himac CP-90α kit (Hitachi, Tokyo, Japan) in the Instrumental Analysis Center at Yeungnam University. After dialysis against PBS, each lipoprotein fraction was equally diluted and pooled.

2.3 Glycation of apoA-I

The purified lipid-free apoA-I (10 mg/mL) was incubated with 250 mM D-fructose in 200 mM potassium phosphate/0.02% sodium azide buffer (pH 7.4) for up to 90 h under gas with air containing 5% CO_2 at 37°C. The extent of advanced glycation reactions was determined from reading the fluorometric intensity at 370 nm (excitation) and 440 nm (emission), as described previously [25].

2.4 Synthesis of rHDL and fluorescence labeling

Reconstituted HDL-containing nA-I or gA-I was prepared via sodium cholate dialysis at a molar ratio of 95:5:1:150

© 2011 WILEY-VCH Verlag GmbH & Co. KGaA, Weinheim

(POPC:cholesterol:apoA-I:sodium cholate), as previously described by our research group [26]. The relevant apolipoproteins and rHDLs were characterized in our previous report [27]. Fluorescent cholesterol derivatives 22-(*N*-7-nitrobenz-2-oxa-1,3-diazol-4-yl)amino-23,24-bisnor-5-cholen-3-ol [NBD-cholesterol, Molecular Probe N-1148, 70 μg of NBD-cholesterol/1 mg of apoA-I] was added to the rHDL.

2.5 Electrophoresis

The same amount of HDL_3 from the elderly and young and apoA-I in the lipid-free and rHDL state were electrophoresed on pre-casted 8–25% native polyacrylamide gradient gels (GE Healthcare, Uppsala, Sweden), using a Pharmacia Phast System (Amersham Pharmacia, Uppsala, Sweden). Sodium dodecyl sulfate-polyacrylamide gel electrophoresis (SDS-PAGE) was carried out according to the method described by Laemmli [28]. IEF was carried out with a pre-casted gel with PhastGel IEF 3–9 (17-0543-01; GE Healthcare) using a PhastSystem (GE Healthcare). The protein bands were visualized by PhastGel Blue R (17-0518-01, GE Healthcare) staining. The range of p*I* for the migrated bands was compared with known p*I* standard proteins, Serva Liquid Mix (Cat. 39212-01, Invitrogen, Carlsbad, CA, USA) containing amyloglucosidase (p$I = 3.6$), β-Lactoglobin (p$I = 5.1$), myoglobin (p$I = 6.6$) and ribonuclease A (p$I = 9.3$).

2.6 Measurement of glycation extent

In order to compare the extent of glycation between the groups, the contents of advanced glycated end products (AGEs) in the individual lipoproteins, including HDL_3 and rHDL, were determined from reading the fluorometric intensities at 370 nm (excitation) and 440 nm (emission), as described previously [29]. A LS55 spectrofluorometer (Perkin-Elmer, Norwalk, CT, USA) was used with WinLab software package version 4.0 (Perkin-Elmer) and a 1-cm path-length suprasil quartz cuvette (Fisher Scientific, Pittsburg, PA, USA).

2.7 Fabrication process of PDMS microchip

The procedure used to make PDMS microchips for IEF is based on a soft lithography technique widely reported in the literature [30]. Briefly, for a pattern replica, a negative photoresist is formed on a Si-wafer substrate using the SU-8 2000 series. The spin rate was controlled and programmed in accordance with the processing guidelines of MICRO-CHEM for the desired channel thickness and coating quality. For the PDMS channel, the PDMS pre-polymer and curing agent (Sylgard 184; Dow Corning, Midland, MI, USA) were uniformly mixed at a ratio of 10:1, and degassed for 2 h at 0.001 tor to remove bubbles inside the PDMS mixture. The PDMS mixture formed on a pattern replica was cured in the oven at 80°C for 4–8 h. After the curing process, the cured PDMS was carefully peeled off from the Si-wafer substrate. The PDMS channel had holes as reservoirs at the end of the channels. The PDMS with a channel pattern and a slide glass for the bottom of the channel were treated by plasma cleaner for 20∼40 s. The microchannel was 2 cm long, 250 μm wide and 25 μm deep.

2.8 Ampholyte-based IEF model

It is very important to achieve a pH gradient with time along the channel length during the IEF process, because the behavior of proteins is significantly changed due to different charge states according to different pH values. Generally, the gel-IEF has non-linear pH curves, whereas the ampholyte-based IEF has step-wise or linear-like pH curves. In addition, the exact p*I* values of the focused proteins can be obtained from the configuration of the pH curves.

In this study, we obtained the pH curves in the ampholyte-based IEF model using the commercial ampholytes and identified the pH curves along the channel. Furthermore, the p*I* point was achieved by comparing the focused positions of proteins and the pH of ampholytes at the same position.

The mathematical model of IEF has been presented in many earlier publications [31, 32]. The ampholyte-based IEF model requires three simultaneous solutions for the mass conservation equations, the charge conservation equation, and the electroneutrality equation for amphoteric molecules. For each amphoteric component, the mass conservation equations without the velocity of bulk flow can be presented, as follows:

$$\frac{\partial C_i}{\partial t} - \nabla \cdot \left[D_i \nabla C_i - (\langle \mu_i \rangle \vec{E}) C_i \right] = 0 \tag{1}$$

where C_i, D_i and $\langle \mu_i \rangle$ are the concentration, diffusion coefficient and effective mobility of component *i*. The electric field, $\vec{E} = -\nabla\phi$, is used in the charge conservation equation

$$\nabla \cdot \left[\nabla \cdot \left(\left[\sum_{i=1}^{N} z_i^2 \omega_i C_i \right] \phi \right) + \sum_{i=1}^{N} D_i \langle z_i \rangle \nabla C_i \right] = 0 \tag{2}$$

where ω_i is absolute mobility, N is the total number of components, including a hydronium and hydroxyl, and $\langle z_i \rangle$ is the effective valence. The concentration of hydronium ions can be found from the electroneutrality condition of the form,

$$\sum_{i=1}^{N-2} \langle z_i \rangle C_i + C_H - \frac{K_w}{C_H} = 0 \tag{3}$$

where C_H is the concentration of hydronium, K_w is the reaction constant of water and N represents all the components, which are proteins, as well as ampholytes, with the exception of hydronium ($C_H \cdot$) and hydroxyl (C_{OH}).

© 2011 WILEY-VCH Verlag GmbH & Co. KGaA, Weinheim

2.9 Assumptions for simulation

The Joule heating becomes disruptive to focusing of the species and affects thermal denaturalization of proteins, as the temperature is higher than 40°C in the channel. Generally, the Joule heating is proportional to conductivity and the square of electric field. In this work, the Joule heating was ignored in this model, because relatively smaller electric fields (50 V/cm) were used and the concentration of proteins was very low for IEF separation, and hence the conductivity was low. Electric field-induced electrokinetic flow was also not considered, because the channel surfaces were coated with methylcellulose to suppress the electro-osmosis flow.

2.10 Boundary conditions

In solving mass conservation equations, the net flux through the channel walls and end wells (reservoirs) are set to zero. The electric potential is subject to insulating boundary conditions $\left(\nabla\phi \cdot \vec{n} = 0\right)$ on the walls, and constant potentials are maintained at the electrode (end) wells. In this study, the electric potential at the anodic well is 50 V, while the potential at the cathodic well is maintained at ground $(\phi_L = 0)$.

2.11 Numerical scheme

The discretized algebraic equations are obtained at each grid point for the mass conservation and modified charge conservation equations. For computational simplicity and stability, structured grids are considered in the simulation. The tridiagonal matrix algorithm (TDMA) [33] is used to solve the discretized algebraic equations along a grid line, and the line-by-line iteration is employed until converged results are obtained throughout the computational domain. The convergence criteria are set as $\left|\frac{C_n - C_{n-1}}{C_n}\right| \leq 10^{-5}$ and $\left|\frac{\phi_n - \phi_{n-1}}{\phi_n}\right| \leq 10^{-5}$ for mass conservation and the charge conservation equation, respectively. The subscripts, n and $n-1$, denote the current and previous iteration steps. In the case of the electroneutrality equation, the Newton–Raphson method [34] was used to obtain the concentration of hydronium ions. Three thousand grid points are used for the microchannel (20 cm × 250 μm × 25 μm (length ×, width × height)). The simulations are performed on an XP-based Samsung computer (Intel(R) Core(TM)2 Quad CPU 2.5 GHz, 1.96 G RAM). The computational time took approximately 3 days for making a stable 31 ampholyte-based pH gradient.

2.12 Data analysis

All data are expressed as the mean ± SD from at least three independent measurements with individual samples. Two-group comparisons were carried by independent *t*-tests using SPSS version 14.0 (SPSS, Chicago, IL, USA). Statistical significance was defined as a $p < 0.05$.

3 Results and discussion

Biomarkers can be widely used to monitor the incidence and progression of disease and the aging process. There have been many papers which have reported putative biomarkers for human aging, as reviewed by Piazza et al. [35], such as telomere length [36] and inflammatory factors [37], including glycation [38].

However, there have been no reports comparing structural and functional changes in serum protein as a biomarker for aging and aging-related disease, such as atherosclerosis and Alzheimer's disease.

In the current study, we compared electromobility of apoA-I in the native or glycated state and HDL_3 from young and elderly groups. Glycated apoA-I-HDL and E-HDL_3 exhibited similar mobility patterns in the lab on a chip which was contributed to by structural modifications due to elevated AGEs. Glycated apoA-I-HDL and E-HDL_3 showed faster mobility in IEF with a broader band range and in microfluidic channels. The faster electromobility was associated with an elevated p*I* of the modified protein.

3.1 Fluorescence of AGEs

Determination of AGEs via the Maillard reaction revealed that fluorescence intensity of glycated apoA-I was 10-fold increased compared to native apoA-I by a 72-h incubation with fructose (final value 250 mM), as shown in Fig. 1A. Under the same protein concentration, isolated HDL_3 from the individuals of elderly group ($n = 26$) showed 15-fold higher intensity ($p < 0.001$) than HDL_3 of the young group ($n = 18$), suggesting that more glycation occurred with age (Fig. 1B).

It has been reported that fructose reacts with proteins at 37°C to produce, via Heyns rearrangement, brown and fluorescent derivatives [39] from a non-enzymatic process called Maillard reaction. After the reaction, the protein qualities can be lowered, due to loss of amino acid residues, altered electrical properties and cross-linking [29].

Our research group reported from fluoroscopic observation that elderly people had a significantly greater extent of protein glycation [15]. The elderly group had 2.3- and 2.9-fold more glycated products in the HDL_2 and HDL_3 fractions in an intact state, respectively, compared with the young group [11]. These results suggest that glycation of HDL and aging are closely associated and might contribute to exacerbation of both pro-inflammatory and pro-atherosclerotic activities.

3.2 Electromobility of HDL

Native apoA-I-rHDL showed a 98–100 Å particle size, while glycated apoA-I-rHDL showed an approximate 93 Å particle size. From three independent electrophoresis experiments, with equally pooled and diluted samples, HDL_3 from the elderly group had a different mobility pattern, with more

© 2011 WILEY-VCH Verlag GmbH & Co. KGaA, Weinheim

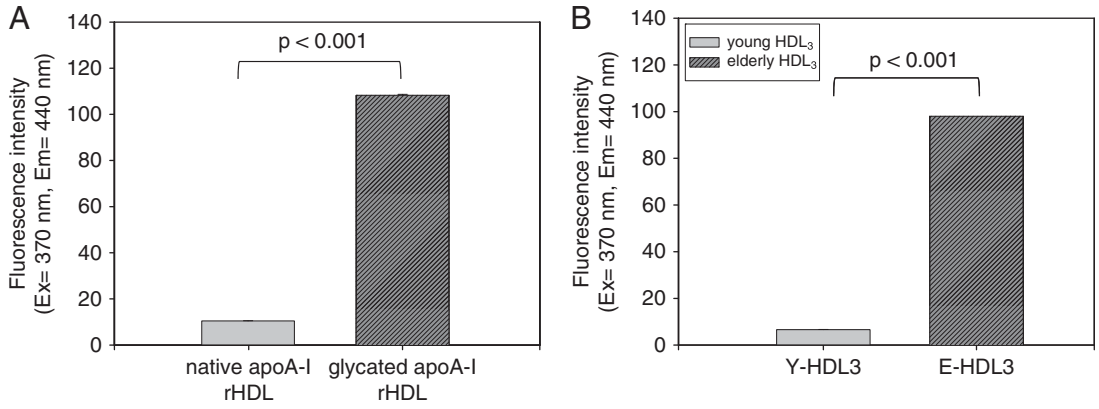

Figure 1. Fluorescence results for the extent of glycation of HDL (Ex = 370 nm, Em = 440 nm). Comparison between the extent of glycation of native and fructosylated apoA-I in rHDL, under the same protein concentration (1 mg/mL). Fructosylation was carried out with 250 mM fructose for 72 h. Comparison of the extent of glycation between young and elderly HDL_3 under the same protein concentration (1.4 mg/mL).

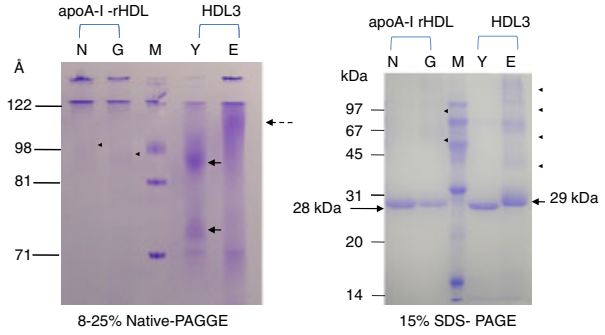

Figure 2. Electrophoretic patterns of apoA-I-rHDL (1 mg/mL of protein) under native (N) and glycated (G) states and HDL_3 (1.4 mg/mL) from young and elderly. Electromobility on 8–25% native-polyacrylamide gradient gel electrophoresis (Native-PAGGE). Electromobility on 15% SDS-PAGE.

aggregates than in the young group (Fig. 2A). Furthermore, young HDL_3 had 3 major bands (91, 74 and 70 Å), whereas E-HDL_3 showed two major bands around 106 and 70 Å, suggesting a different subtype. SDS-PAGE analysis revealed that glycated apoA-I showed an increased smear band intensity with a multimerization pattern (indicated by the arrow head), compared to native apoA-I. Similarly, HDL_3 from the elderly had increased multimerized apoA-I with faint and smear intensity, whereas HDL_3 from the young group had distinct band intensity (Fig. 2B). Furthermore, in three independent electrophoresis experiments with equally pooled and diluted samples, apoA-I from the elderly had a higher band position, suggesting that the electromobility of HDL_3 was altered by aging.

3.3 IEF on polyacrylamide gel

As shown in Fig. 3, glycated apoA-I rHDL migrated on the IEF gel (pH 3–10) in the more basic region to the bottom, with increased faint intensity, compared with nA-I-rHDL. In addition, native apoA-I-rHDL showed more distinct band intensity and less mobility to the bottom, suggesting that it had a lower p*I* than glycated rHDL. E-HDL_3 had a broader band range than Y-HDL_3 with more smear band intensity, indicating a relatively broader isoelectric point value range. Glycated rHDL and E-HDL_3 migrated more to the bottom of the gel with a broader area of diffusion. The band migration was quantified and calculated p*I* range was provided after comparison with known pI standard proteins Serva Liquid Mix (Cat. 39212-01, InVitrogen) as shown in inset table.

The elevated p*I* was associated with fructosylation of protein to produce AGEs. The initial phase of the Maillard reaction with fructose occurred at either the α-amino or ε-amino groups of Lys residues, via Heyns rearrangement [40]. ApoA-I has 21 Lys residues in the primary sequence of 243 amino acids. Recently, our research group reported that fructosylated apoA-I, both in lipid-free and lipid-bound states, failed multimerization in the presence of a cross-linker [bis(sulfosuccinimidyl) suberate BS_3], which was reactive to the ε-amino group of Lys [41]. Without cross-linker-induced multimerization, the fructosylated apoA-I and apoA-I in E-HDL showed spontaneous multimerization, with increased molecular weight and smear band intensity on 15% SDS-PAGE. These results suggest fructose adduct formation and fructose-mediated spontaneous multimerization in serum proteins, which is well known in albumin and hemoglobin [42, 43].

3.4 IEF in microchannels and simulation

An ampholyte-based IEF simulation was conducted to obtain the pH gradient in a straight channel. This mathematical model is based on the mass conservation and ionic dissociation relationships of amphoteric macromolecules, charge conservation and the neutral electrical condition. Based on the 2-D model, 31 ampholytes were

© 2011 WILEY-VCH Verlag GmbH & Co. KGaA, Weinheim

used in the pH range of 3.5–9.5 ($\Delta pI = 0.2$, $\Delta pk = 1$). The ionic mobility was $3 \times 10^{-8}\,m^2/V\,s$ and the normalized initial concentrations were used for ampholytes. The 50 V electrical potential was applied to the anode (right side), while zero electrical potential was maintained at the cathode (left side). In Fig. 4, normalized concentration behaviors during the IEF process are plotted for ampholytes. Initially, the concentrations of all ampholytes were uniformly distributed along the channel. The concentrations simultaneously evolved at the anode and cathode. Two peaks of each concentration occurred and moved to the center of the channel (Fig. 4A and B). The 31 ampholytes stopped at the p*I* points and focused until reaching a steady-state condition (Fig. 4C). At approximately 1000 s, the 40-fold concentrations are made in the steady-state condition (Fig. 4C). The pH profiles are shown during the IEF process (Fig. 5). In order to determine the p*I* value, the focused position of the protein from the experiments should be compared from the pH value versus position in Fig. 5. Initially, the pH was flat along the channel due to the same concentrations of ampholytes. However, as the concentrations of ampholytes increased at both the anode and cathode, the pH had a sharp gradient at 50 s. The 31 ampholytes are sufficient to make a linear pH gradient, whereas small ampholytes

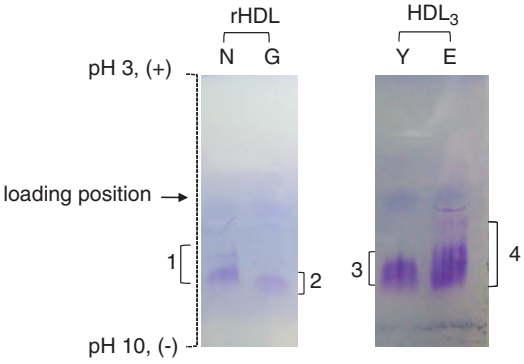

Migrated band #	pI range
1. Native (N) apoA-I rHDL	6.9 – 7.8
2. Glycated (G) apoA-I rHDL	7.8 – 8.1
3. Young (Y) HDL_3	7.2 – 7.9
4. Elderly (E) HDL_3	6.2 – 8.3

Figure 3. Electromobility of apoA-I-rHDL (1 mg/mL of protein) under native and glycated states and HDL_3 (1.4 mg/mL) from young and elderly on IEF gel (pH 3–10). N, native state; G, glycated state; Y, young; E, elderly. The inset table shows calculated p*I* range after comparison with known p*I* standard proteins as described in Section 2.

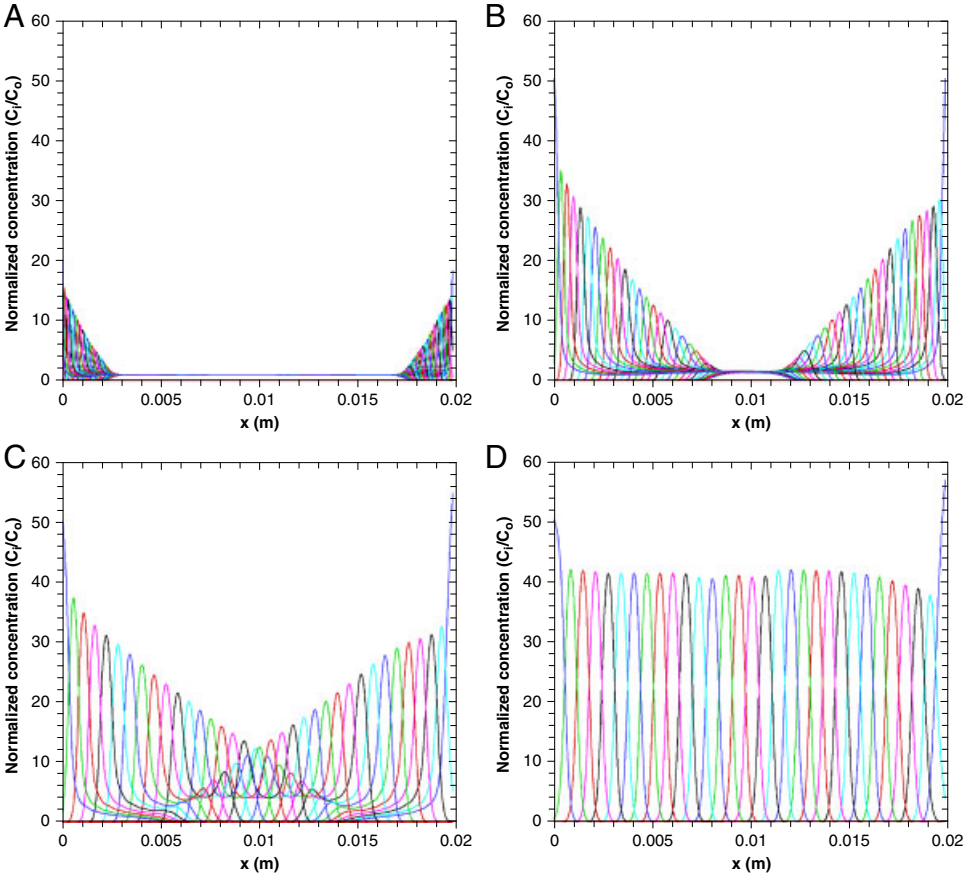

Figure 4. Normalized concentration behavior of ampholytes during the IEF process: (A) 50 s, (B) 200 s, (C) 400 s and (D) 1000 s.

© 2011 WILEY-VCH Verlag GmbH & Co. KGaA, Weinheim

make a step-wise gradient. It was shown that the pH profile is made as ampholytes change at 100∼400 s. The pH profiles are not significantly changed close to the steady-state time ($t = 1000$ s). We conclude that the linear pH gradient was made for 31 ampholytes over a pH range of 3.5–9.5 ($\Delta pI = 0.2$, $\Delta pk = 1$) and was able to identify p*I* points of proteins according to the channel length.

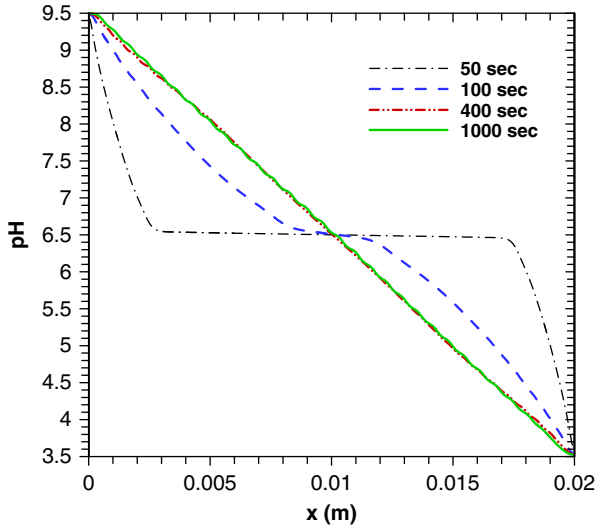

Figure 5. Changes in the pH distribution during the ampholytes-based IEF process under the electric potential of 50 V, with 31 ampholytes

3.5 Electromobility in the microfluidic channel

After 25 min in electromigration, native apoA-I-NBD-rHDL (26 ng of apoA-I and 0.8 ng of NBD in channel) showed a more condensed band migration pattern, with more distinct green fluorescence, whereas glycated apoA-I-rHDL showed a scattered band pattern, with weaker fluorescence, as shown in Fig. 6A and B. Similarly, Y-HDL_3 showed a more condensed band pattern with stronger fluorescence intensity, whereas E-HDL_3 showed a much broader band migration with less intensity (Fig. 7A and B). During electrophoresis, we could not find protein absorption in the PDMS channel.

In order to determine the p*I* value, the focused position of the protein from the experiments should be compared from the pH value versus position in Fig. 5. From the p*I* determination based on the titration curve, the p*I*s of native apoA-I-rHDL and glycated apoA-I rHDL were 6.2 ± 0.2 and 7.0 ± 0.2, respectively (Fig. 6C and D). The pIs of Y-HDL_3 and E-HDL_3 were 6.9 ± 0.5 and 8.1 ± 0.5, respectively (Fig. 7C and D). These results suggest that glycation could cause an increase in p*I* with a broader range, which correlates well with data from the IEF gel (Fig. 3).

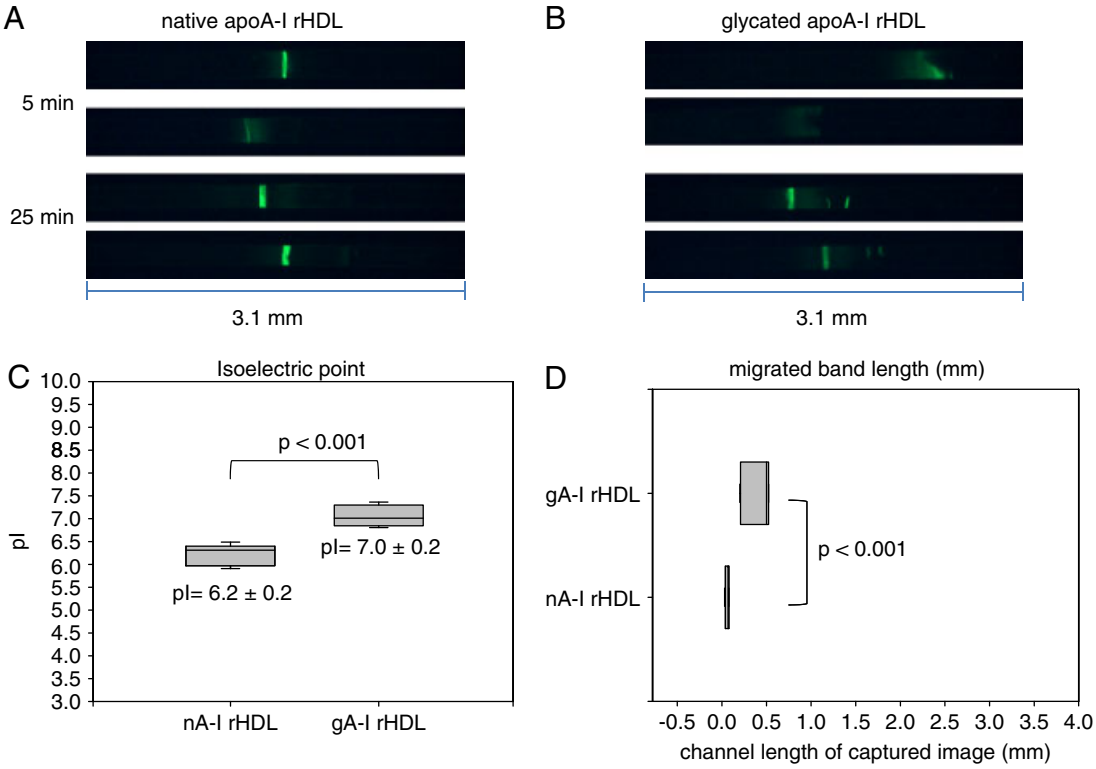

Figure 6. Representative image of apoA-I-rHDL migration in microfluidic channel, in the presence f ampholyte (pH 3–10). Fluorescence image of the migration pattern at 5 min (A) and 25 min (B). The distance of migration (C) and p*I* range (D) determined from the computational simulation model.

© 2011 WILEY-VCH Verlag GmbH & Co. KGaA, Weinheim

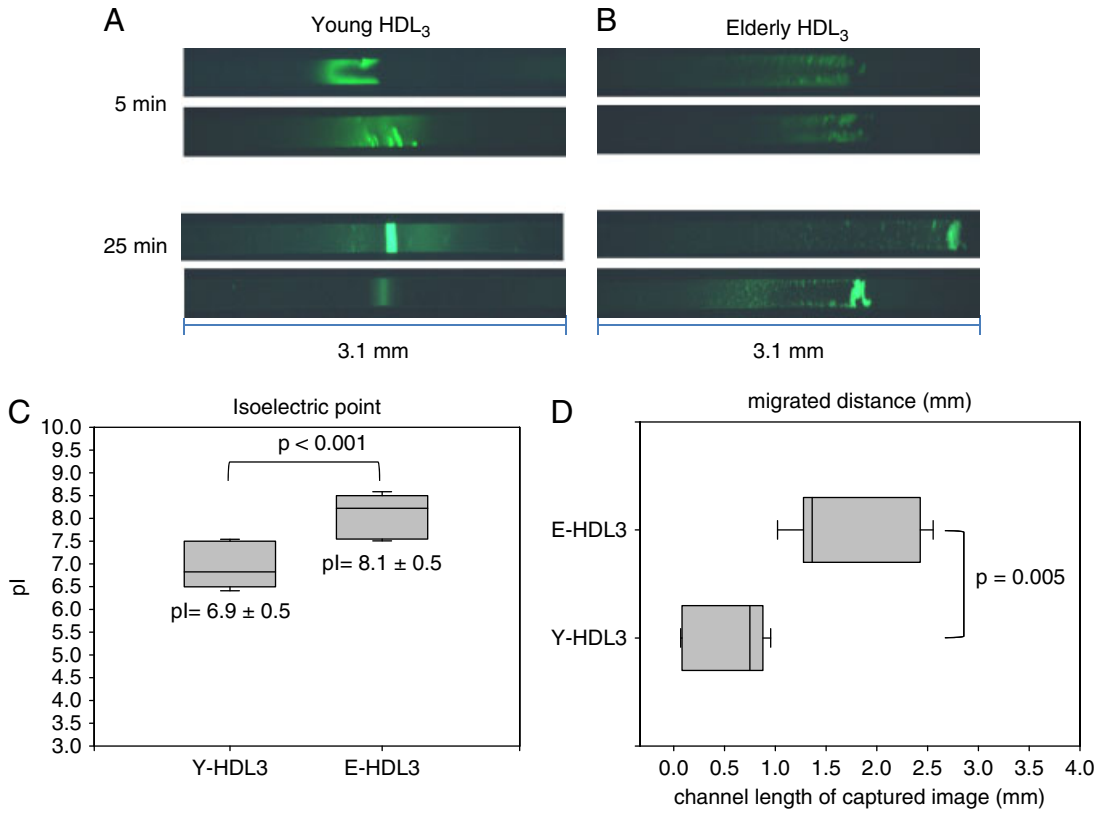

Figure 7. Representative image of migrated pattern of HDL_3 from young or elderly in microfluidic channel in the presence of ampholyte (pH 3–10). Fluorescence image of migration pattern at 5 min (A) and 25 min (B). The distance of migration (C) and p*I* range (D) determined from the computational simulation model.

Glycated apoA-I-rHDL and E-HDL had faster migration speeds in the channel than native apoA-I and Y-HDL (data not shown). In addition, gA-I-rHDL had a longer band scattering pattern (0.4 ± 0.1 mm) than nA-I-rHDL (0.06 ± 0.02 mm). Similarly, E-HDL_3 had a longer band scattering pattern (1.7 ± 0.6 mm) than Y-HDL_3 (0.5 ± 0.4 mm). These results suggest that glycation of protein in HDL could modify both the p*I* value and electromobility in the microfluidic channel.

Lab on a chip analysis is a miniaturization of chromatography and electrophoresis, with considerable interest for monitoring biomarkers. Glycated apoA-I-rHDL and E-HDL lost anti-atherosclerotic and antioxidant properties and showed enhanced cellular influx of cholesterol [11]. Based on IEF, we developed a method to detect modified HDLs in a microfluidic channel, which may be useful for diagnosing the extent of senescence. Similarly, a PDMS chip is widely used to monitor the progress of metabolic disease, such as type 2-diabetes [44]. Although current biomarkers for aging are related to the telomere length, it is necessary to find a new serum protein marker to develop a convenient and non-invasive method.

Interestingly, E-HDL and glycated HDL shared several physical characteristics, i.e. increase in AGEs, a change to a more basic isoelectric point, multimerized tendency of apoA-I, and faster mobility in IEF and microfluidic channels. Glycated apoA-I and E-HDL_3 also showed similar properties; specifically, an elevated level of non-tryptophan Maillard fluorescence (Fig. 1), spontaneous multimerization (Fig. 2), increased p*I* (Fig. 3), and faster electromobility (Figs. 5–7) were demonstrated in both compounds.

In the current study, we have shown that apoA-I and HDL can be modified by aging and glycation, which can display characteristics of biomarker for aging. Monitoring of the modification of HDL using lab on a chip can be a rapid and reliable diagnostic tool for the extent of aging and onset of aging-related disease. These detection methods can be applied to develop a new biosensor for point of care, which is available for handheld usage and onsite analysis.

4 Concluding remarks

Reconstituted HDL containing glycated apoA-I and HDL from elderly share several electrophoretic properties with multimerization and faster mobility in microfluidic channels, which depends on the ampholyte-based isoelectric focusing. These results can be applied to develop a rapid detection system for modified HDL to predict the extent of senescence and onset of aging related diseases, such as cardiovascular disease, diabetes and dementia.

© 2011 WILEY-VCH Verlag GmbH & Co. KGaA, Weinheim

This work was supported by the Mid-career Researcher Program (2011-0015529), Basic Science Researcher Program (2010-0020910), and Aging-associated Vascular Disease Research Center at Yeungnam University (R13-2005-005-01003-0 [2011]) through the National Research Foundation of Korea (NRF) by the Ministry of Education, Science and Technology (MEST).

The authors have declared no conflict of interest.

5 References

[1] Gordon, T., Castelli, W. P., Hjortland, M. C., Kannel, W. B., Dawber, T. R., *Am. J. Med.* 1977, *62*, 707–714.

[2] Fielding, C. J., Fielding, P. E., *J. Lipid Res.* 1995, *36*, 211–228.

[3] Lee, H., Park, J. E., Choi, I., Cho, K. H., *BMB Rep.* 2009, *42*, 605–610.

[4] Arai, Y., Hirose, N., *J. Atheroscler. Thromb.* 2004, *11*, 246–252.

[5] Nikkila, M., Heikkinen, J., *Age Ageing.* 1990, *19*, 119–124.

[6] Koropatnick, T. A., Kimbell, J., Chen, R., Grove, J. S., Donlon, T. A., Masaki, K. H., Rodriguez, B. L., Willcox, B. J., Yano, K., Curb, J. D., *J. Gerontol. A Biol. Sci. Med. Sci.* 2008, *63*, 1235–1240.

[7] Toth, P. P., Davidson, M. H., *J. Clin. Lipidol.* 2010, *4*, 359–364.

[8] Nobécourt, E., Tabet, F., Lambert, G., Puranik, R., Bao, S., Yan, L., Davies, M. J., Brown, B. E., Jenkin, A. J., Dusting, G. J., Bonnet, D. J., Curtiss, L. K., Barter, P. J., Rye, K. A., *Arterioscler. Thromb. Vasc. Biol.* 2010, *30*, 766–772.

[9] Robbesyn, F., Augé, N., Vindis, C., Cantero, A. V., Barbaras, R., Negre-Salvayre, A., Salvayre, R., *Arterioscler. Thromb. Vasc. Biol.* 2005, *25*, 1206–1212.

[10] Khalil, A., Jay-Gerin, J. P., Fülöp, T., Jr., *FEBS Lett.* 1998, *435*, 153–158.

[11] Park, K. H., Cho, K. H., *J. Gerontol. A Biol. Sci. Med. Sci.* 2011, *66*, 511–520.

[12] Yoshikawa, M., Sakuma, N., Hibino, T., Sato, T., Fujinami, T., *Clin. Biochem.* 1997, *30*, 221–225.

[13] Cho, K. H., Park, S. H., Park, J. E., Kim, Y. O., Choi, I., Kim, J. J., Kim, J. R., *Clin. Biochem.* 2008, *41*, 56–64.

[14] Park, K. H., Shin, D. G., Kim, J. R., Hong, J. H., Cho, K. H., *Int. J. Mol. Med.* 2010, *25*, 129–136.

[15] Park, K. H., Shin, D. G., Kim, J. R., Cho, K. H., *J. Gerontol. A. Biol. Sci. Med. Sci.* 2010, *65*, 600–610.

[16] Tan, W., Fan, Z. H., Qiu, C. X., Ricco, A. J., Gibbons, I., *Electrophoresis* 2002, *23*, 3638–3645.

[17] Sia, S. K., Whitesides, G. M., *Electrophoresis* 2003, *24*, 3563–3576.

[18] Li, Y., Buch, J. S., Rosenberger, F., DeVoe, D. L., Lee, C. S., *Anal. Chem.* 2004, *76*, 742–748.

[19] Shimura, K., *Electrophoresis* 2009, *30*, 11–28.

[20] Subirats, X., Blaas, D., Kenndler, E., *Electrophoresis* 2011, *32*, 1579–1590.

[21] Chong, C. P., Lin, T. Y., Chang, C. L., Yang, Y. L., Tsai, M. H., Yu, Y. S., Liu, M. Y., *Electrophoresis* 2011, *32*, 1241–1251.

[22] Brewer, H. B., Jr., Ronan, R., Meng, M., Bishop, C., *Methods Enzymol.* 1986, *128*, 223–246.

[23] Lee, H., Cho, K. H., *Int. J. Mol. Med.* 2011, *27*, 841–849.

[24] Havel, R. J., Eder, H. A., Bragdon, J. H., *J. Clin. Invest.* 1955, *34*, 1345–1353.

[25] McPherson, J. D., Shilton, B. H., Walton, D. J., *Biochemistry* 1988, *27*, 1901–1907.

[26] Cho, K. H., Park, S. H., Han, J. M., Kim, H. C., Choi, Y. K., Choi, I., *Eur. J. Clin. Invest.* 2006, *36*, 875–882.

[27] Cho, K. H., *Mol. Cells* 2009, *27*, 291–297.

[28] Laemmli, U. K., *Nature* 1970, *227*, 680–685.

[29] Pongor, S., Ulrich, P. C., Bencsath, F. A., Cerami, A., *Proc. Natl. Acad. Sci. USA* 1984, *81*, 2684–2688.

[30] Cui, H., Dutta, P., Ivory, C. F., *Electrophoresis* 2007, *28*, 1138–1145.

[31] Shim, J., Dutta, P., Ivory, C. F., *Electrophoresis* 2007, *28*, 572–586.

[32] Shim, J., Dutta, P., Ivory, C. F., *Electrophoresis* 2008, *29*, 1026–1035.

[33] Patankar, S. V., *Numerical Heat Transfer and Fluid Flow*, Hemisphere Publishing Corp., New York 1980.

[34] Burden, R. L., Faires, J. D., *Numerical Analysis*, 8th Edn., Brooks/Cole, Boston 2005.

[35] Piazza, J. R., Almeida, D. M., Dmitrieva, N. O., Klein, L. C., *J. Gerontol. B Psychol. Sci. Soc. Sci.* 2010, *65*, 513–525.

[36] Butler, R. N., Sprott, R., Warner, H., Bland, J., Feuers, R., Forster, M., Fillit, H., Harman, S. M., Hewitt, M., Hyman, M., Johnson, K., Kligman, E., McClearn, G., Nelson, J., Richardson, A., Sonntag, W., Weindruch, R., Wolf, N., *J. Gerontol. A Biol. Sci. Med. Sci.* 2004, *59*, B560–B567.

[37] Alonso-Fernández, P., De la Fuente, M., *Curr. Aging Sci.* 2011, *23*, 78–100.

[38] Ansari, N. A., Moinuddin, Ali. R., *Dis. Markers* 2011, *30*, 317–324.

[39] Dills, W. L., Jr., *Am. J. Clin. Nutr.* 1993, *58*, 779S–787S.

[40] Schalkwijk, C. G., Stehouwer, C. D., van Hinsbergh, V. W., *Diabetes. Metab. Res. Rev.* 2004, *20*, 369–382.

[41] Park, K. H., Jang, W., Kim, K. Y., Kim, J. R., Cho, K. H., *Biochem. Biophys. Res. Commun.* 2010, *392*, 295–300.

[42] Tan, K. C., Chow, W. S., Ai, V. H., Metz, C., Bucala, R., Lam, K. S., *Diabetes Care* 2002, *25*, 1055–1059.

[43] Bantle, J. P., *J. Nutr.* 2009, *139*, 1263S–1268S.

[44] Oblak, T. D., Meyer, J. A., Spence, D. M., *Analyst* 2009, *134*, 188–193.

© 2011 WILEY-VCH Verlag GmbH & Co. KGaA, Weinheim